applied sciences

MDPI

Article

Influence of Pre-Strain and Notching on the Fatigue Life of DD11 Low-Carbon Steel

Ivan Tomasi [1,†], Luigi Solazzi [1,*,†], Candida Petrogalli [1,†], Alberto Mazzoni [2,†] and Giorgio Donzella [1,†]

[1] DIMI Department, University of Brescia, Via Branze 38, 25123 Brescia, Italy; ivan.tomasi@unibs.it (I.T.); candida.petrogalli@unibs.it (C.P.); giorgio.donzella@unibs.it (G.D.)
[2] Moveero R&D Centre Europe, Via Molino Emili 18, 25030 Brescia, Italy; alberto.mazzoni@moveero.com
* Correspondence: luigi.solazzi@unibs.it
† These authors contributed equally to this work.

Abstract

Structural applications commonly adopt low-carbon steels, with the fatigue concept being one of the primary causes of failure. In this research, the aim was to study the fatigue behaviour of DD11 low-carbon steel, considering also specific conditions, like the effect of pre-deformation and influence of stress intensity factor. After determining the geometry and performing static tests to extrapolate the mechanical properties of the material, the fatigue behaviour of the base material was analysed, following the actual standards. Then, two conditions, a pre-strain equal to 11% and a notch, simulated with a hole and without pre-deformation, were studied. The results showed an absence of influence on the fatigue limit for the material with a pre-strain effect, and regarding the notching tests conducted, there was a low sensitivity to fatigue of the material.

Keywords: fatigue; rolled steel; experimental tests; numerical analysis

Academic Editor: Andrea Carpinteri

Received: 18 July 2025
Revised: 2 September 2025
Accepted: 8 September 2025
Published: 9 September 2025

Citation: Tomasi, I.; Solazzi, L.; Petrogalli, C.; Mazzoni, A.; Donzella, G. Influence of Pre-Strain and Notching on the Fatigue Life of DD11 Low-Carbon Steel. *Appl. Sci.* **2025**, *15*, 9886. https://doi.org/10.3390/app15189886

1. Introduction

The fatigue life of a component has always been difficult to predict due to the multiplicity of variables that are involved in the process. This phenomenon affects several industrial fields, such as automotive [1,2], lifting equipment [3,4], but also pressure vessels [5] or railway vehicles [6]. In all these fields, steel is one of the most adopted families of materials due to multiple factors, for example, its mechanical properties, its reliability or the vast knowledge about its behaviour. Low-carbon steel, a good compromise between mechanical properties and processing aptitude, is a widely used material in this family.

Regarding the fatigue behaviour of these materials, there are several studies concerning both low-cycle fatigue (LCF) [7] and high-cycle fatigue (HCF) [8], but also concerning the particular situation of the material: Kim et al. [9] analysed the fatigue behaviour of a low-carbon steel and the fatigue behaviour of welded joints obtained through the plasma arc welding process; the authors found that the cyclic stress response in the HCF mode showed an initial cyclic softening, followed by cyclic stabilisation, while for the welded joints, the extremely low cycle fatigue (ELCF) mode at large strains showed no cyclic stabilisation after initial cyclic hardening. Tsutsumi et al. [10] analysed the very high cycle fatigue (VHCF) through ultrasonic fatigue tests (20 kHz) of annealed and 10% pre-strained specimens for 0.13% carbon steel, discovering that fatigue lives and fatigue limits under these conditions were higher than those under conventional tension–compression fatigue tests. Mayer [11] studies concerned the differences between the fatigue limits with constant

amplitude and two-step variable amplitude, finding that two-step variable amplitude endurance and fatigue crack growth experiments could show detrimental or beneficial influences of low-load cycles on fatigue damage, and the maximum load amplitude of the variable amplitude repeat sequence determined which effect prevailed. Regarding the effect of pre-strain on the tensile and fatigue strength of low-carbon steel, several studies have been reported, but always regarding low-carbon steels with high strength due to their particular production processes or chemical compositions [12–14], or observing the effect of heat treatments [15]. Regarding the effect of notching, the main studies [16] analyse the stress concentration factor when the stress ratio R = −1, but not many studies consider other values of R. Another research study conducted by Liao et al. [17] highlights the possible factors which influence the fatigue notch factor K_f, pointing out that different stress ratios also produce different values of K_f. Zhang et al. [18,19] investigated the effect of multiple corrosion pits on high-strength steel wires and the influence of their geometric parameters on the stress concentration factor of those materials, also developing innovative models to predict the fatigue life of steel bridge decks' welds based on machine learning approaches [20].

However, in the literature, limited works have been reported pertaining to the influence of pre-strain or notching on the behaviour of low-carbon, hot-rolled mild steel subjected to cyclic loads with $R \neq -1$, especially if the loads bring the material over the yield strength.

With this in mind, this research article analyses the influence of pre-strain and notching on the fatigue life of low-carbon steel (DD11) through several experimental tests, which can give useful additional information about the fatigue material properties in real industrial applications, for example, agricultural or industrial wheels [21], where DD11 steel is widely use for the rim manufacturing [22]. In fact, after the production process, this component has areas either plastically deformed or with notches, like the valve hole, which are subjected to cyclic load during service. An example of this application can be seen in Figure 1.

Figure 1. Example of an engineering application of the studied material. In agricultural wheels, the part of the wheel called rim is deformed plastically, and the tyre valve defines a dangerous notch which can reduce the material strength.

In this study, after a general presentation of the material characteristics, the focus is put on the geometry of the specimens (Section 2). Then, the test machines used and the procedures followed for the tensile and fatigue testing are presented in detail (Section 3).

In Section 4, a finite element (FE) model developed for a numerical simulation of the tests is introduced. It is used as a further verification of the experimental results from the lab testing, analysing the stress distribution in the gauge area of the specimens and around the notch. It is further highlighted in Section 5, where the overall results of tensile and fatigue testing are presented and discussed in detail, also in reference to the FEA results. A low sensitivity of the material to high pre-strain is found. Regarding the notch effect, outcomes also show a lower sensitivity of the material than theoretical calculations, due to a local plasticisation of the material around the notch itself. Reasons for that are discussed in detail and the overall results are then summarized in Section 6, where future developments of this research are also suggested.

2. Material and Specimens

In the current study, the specimen material was DD11 low-carbon steel (1.0332 to the UNI EN 10027-2:2015 standard [23]). According to the UNI EN 10111:2008 standard [24], Table 1 shows the chemical composition of the material, while the mechanical properties are shown and discussed in Section 5.1. The specimens were obtained with the longest dimension perpendicular to the rolling direction. This means a different behaviour compared to the longitudinal direction due to the manufacturing process of the material. The location of the material samples from the original strip was chosen in accordance with ISO 377:2017 [25].

Table 1. Chemical composition of DD11 steel (wt%).

C	Mn	P	S	Si	Al	Cu	Ni	Cr	N
0.07	0.42	0.010	0.008	0.05	0.016	0.030	0.012	0.020	0.004

All of the specimens used in this work were characterised by a flat geometry and featured a rectangular cross section; in fact, they were directly machined from a hot-rolled DD11 steel sheet, as can be seen in Figure 2.

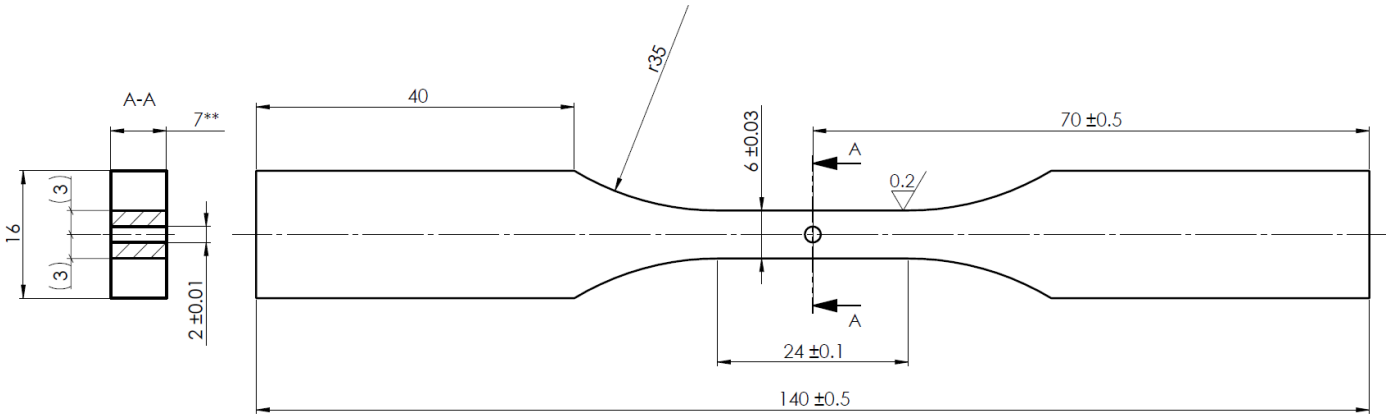

Figure 2. Technical drawing of notch specimen: for the smooth specimen, the gauge section is 4 × 7 mm, and it does not include the 2 mm diameter hole, whereas here, it is 6 × 7 mm due to the presence of the hole. The radius *r* of the transition area in the notch specimen is 35 mm, whereas in the smooth specimen, it is 30 mm. The thickness of the specimen is equal to 7 mm and the symbol ** indicates it comes directly from the hot-rolled coil, where the tolerance follows the UNI EN 10051 standard [26].

Overall, two types of specimens were produced: smooth and notched; Figure 3 illustrates their geometries. This geometry was chosen to satisfy the following:

- International standards for both tensile tests and fatigue tests (respectively, ISO 6892-1 [27] and ISO 12107:2012 [28]);

- Specifications of the test machines;
- Base material strip, which had a nominal thickness of 7 mm (in Figure 2, it can be seen in section A-A).

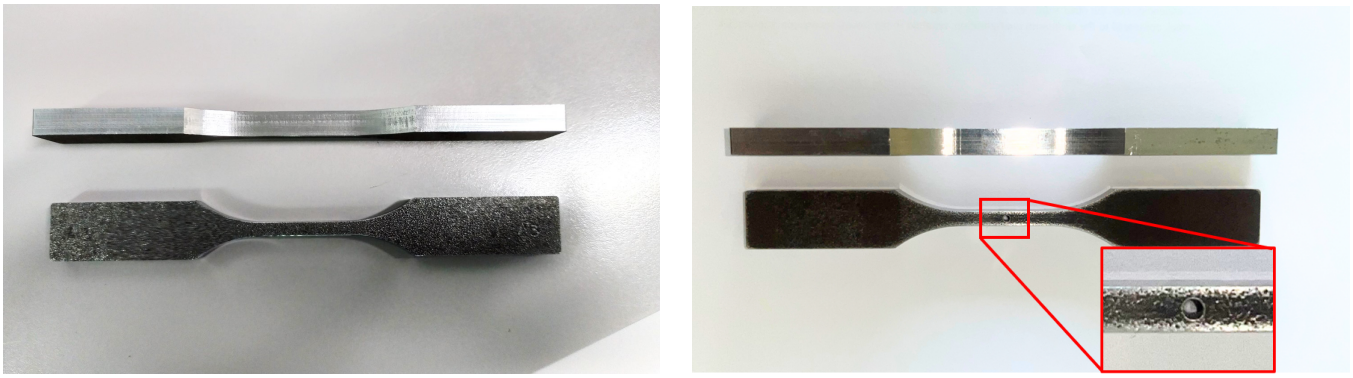

(**a**) (**b**)

Figure 3. Photos of the specimens adopted: here, it can be noticed that the specimens were obtained directly from the coil strip through milling. (**a**) Smooth specimen. (**b**) Notched specimen, with a zoom to highlight the presence of the hole.

3. Experimental Analysis

3.1. Test Machines for Tensile Tests and for Uniaxial Fatigue Tests

Regarding the test machines used, the servo-hydraulic universal testing machine Instron 8501 with a maximum load capacity of 100 kN was adopted for the tensile tests on the material, while for the fatigue tests, the Rumul Mikrotron resonant machine (Russenberger Prüfmaschinen AG, Neuhausen am Rheinfall, Switzerland) with a maximum load capacity of 20 kN was utilized, as shown in Figure 4.

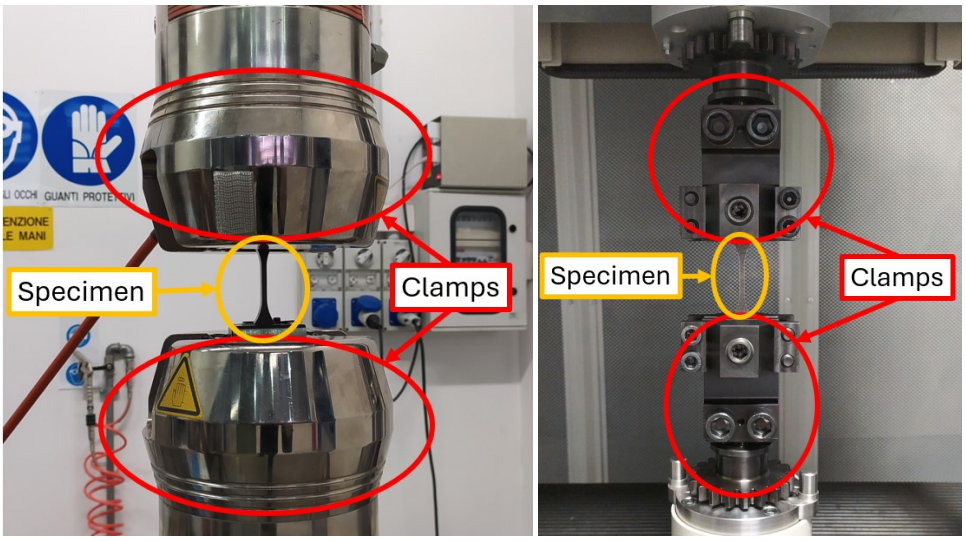

(**a**) (**b**)

Figure 4. Photos of the experimental test machines. (**a**) Tensile test setup, where the clamps work through a servo-hydraulic system. (**b**) Fatigue test setup, where the clamps work through a mechanical system.

3.2. Tensile Tests

Before analysing the fatigue behaviour of the material, uniaxial tensile tests must be conducted with the aim of a better comprehension of the behaviour of the material, as they allow for a physical interpretation of the stress values. Furthermore, the fatigue strength of

the material could be estimated as a first approximation from the tensile strength [29] for an appropriate choice of load levels.

The tensile tests were performed on the tensile testing machine in displacement control, as the transverse speed was set to 2 mm/min, falling within the range specified by ISO 6892-1 [27], which states that the transverse speed must be between 1 mm/min and 5 mm/min. An extensometer was installed on the gauge area of the specimens (see Figure 5a) with the purpose of recording accurate deformation data for the linear–elastic region where the estimation of the Young modulus had to be made. However, it was decided to remove the extensometer after reaching a displacement of 0.15 mm; the choice of this parameter was guided by an earlier estimation of the elastic region.

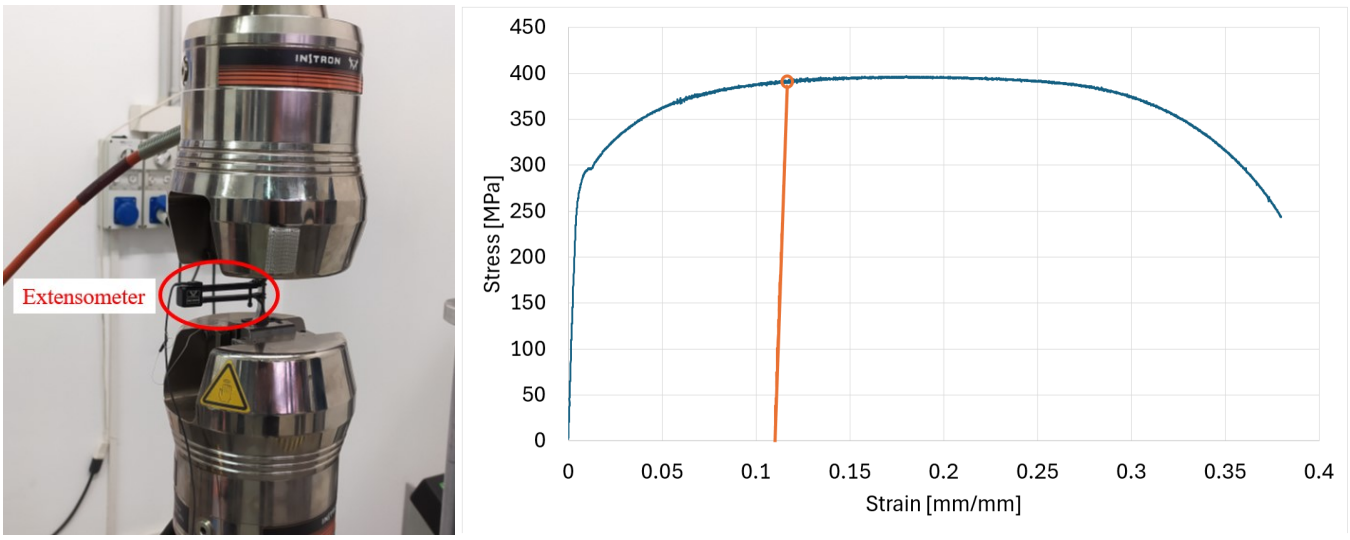

(**a**) (**b**)

Figure 5. Tensile test with an extensometer and stress–strain result. (**a**) Image of the extensometer, directly applied to the specimen. (**b**) Stress–strain chart of the material, highlighting the level of pre-strain analysed.

3.3. Fatigue Tests

In this research, axial fatigue tests were performed at a frequency of ca. 80 Hz, with load ratio R = 0.1 (except for two series of tests where the load ratio was R = 0.01 and R = 0.2) and a sinusoidal load function. The reason for these particular load ratio values was driven by the need to avoid compression and by a limitation on maximum stress to maintain the same failure mode and stay away from the LCF field; moreover, considering one of the applications of this material shown previously, the load ratios chosen also matched the classic stress behaviour of agricultural wheels.

As the failure criterion, the complete fracture of the specimen was assumed. Nevertheless, if specimens reached 2,000,000 cycles, the tests were stopped and considered runouts. The reason for this specific number was its extensive use in literature (examples are [30–32]). In this study, different conditions were analysed:

- Fatigue behaviour of the material through different stress ratios, defining a Wohler's curve.
- Fatigue limit of the material with an 11% pre-strain level, through the staircase method. A similar value of pre-strain was already investigated in the literature with a similar material [33]. To understand this percentage, Figure 5b shows this pre-deformation on the stress–strain graph of the material.
- The fatigue limit of the material, considering the notch effect, was determined using the staircase method.

To understand the staircase method, the example of the base material with R = 0.1 is reported in Tables 2 and 3. A staircase method is usually defined by a minimum of 15 specimens, but having described the whole curve for the base material, it was possible to adopt only 6 specimens according to the UNI ISO 3800 standard [34], which is based on the homoscedasticity hypothesis, i.e., that the standard deviations of both fatigue limit and finite life region are the same. Here, 11 tests are shown to validate the hypothesis previously made.

Table 2. Staircase test procedure of the base-material C specimens.

σ_a	Specimen ID										
[MPa]	**R1.1**	**R1.2**	**R1.3**	**R1.4**	**R1.5**	**R1.6**	**R1.7**	**R1.8**	**R1.9**	**R1.10**	**R1.11**
145			X		X				X		X
142.5		O		O		X		O		O	
140	O						O				

Table 3. Evaluation of the fatigue limit of the notched PS specimens.

Stress [MPa]	**Level**	**Events**		**Values**		
S_i	i	**X**	**O**	f_i	if_i	i^2f_i
145	2	4	0	4	8	16
142.5	1	1	4	1	1	1
140	0	0	2	0	0	0
Sum	-	5	6	$C = 5$	$A = 9$	$B = 17$

Table 2 shows the tests for the staircase method, their amplitude stress, and whether the test was a runout (marked with "O") or whether the specimen reached failure (marked with "X"). In this method, each test is dependent on the previous, so if the previous specimen fails, the new test should be taken to a lower level of stress amplitude and vice versa; if a previous specimen is a runout, the new test should be taken to an upper level of stress amplitude. Table 3 elaborates the results: the level starts as zero, the lowest level of stress amplitude (in this scenario, 140 MPa), and the values to evaluate coefficients C, A and B are taken based on the least number of events, so here, the failure tests ("X") are chosen as being less than the runouts. Coefficient C is the sum of the events chosen, coefficient A is the sum of each event multiplied by its level of stress amplitude, while coefficient B is the sum of each event multiplied by the square of its level of stress amplitude. These coefficients are needed to evaluate the fatigue limit σ_{a50} and its standard deviation ($Std.Dev.$) through Equation (1) [34]:

$$\sigma_{a50} = \sigma_0 + \Delta S\left(\frac{A}{C} \pm 0.5\right); \quad Std.Dev. = 1.62 \cdot \Delta S\left(\frac{C \cdot E - A^2}{C^2} + 0.029\right) \tag{1}$$

where σ_0 is the lowest level of stress amplitude of the staircase method, ΔS is the step level of the stress amplitude (in this case chosen equal to 2.5 MPa), and the sign before the value 0.5 in Equation (1) depends on the analysed event: a minus sign if the analysed events are tests reaching failure or plus sign if they are runouts.

Table 4 shows the alphanumeric coding used to label the specimens implemented in this research work. For the tensile tests, specimens labelled with the letter T were implemented. To define the fatigue behaviour of the material, R1, R2, R01 specimens were used, while for investigating the fatigue limit of the material with pre-deformation,

specimens labelled with PS were adopted. To investigate the notch effect, specimens with the letter N were used.

Table 4. Legend of the letters used for specimen identification.

ID	#	Purpose
T	3	Tensile tests on the base material
R1	26	Fatigue tests on the base material at $R = 0.1$
R2	15	Fatigue tests on the base material at $R = 0.2$
R01	15	Fatigue tests on the base material at $R = 0.01$
PS	15	Fatigue tests on axially deformed specimens ($\epsilon_p = 11\%$)
N	15	Fatigue tests on notched specimens

It must be highlighted that positive values of load ratios were chosen to avoid a possible buckling effect, which can happen with a negative load ratio due to the contribution of the compression. Another reason of such load ratios lay in one of its mechanical applications: considering the agricultural wheel, there is a mean stress due to the pressure of the tyre, and an alternate stress due to the rotation of the wheel itself. The reason for the different load ratios for R01 specimens is that studying the fatigue with different load ratios makes it possible to define the entire Wohler's curve of the material, i.e., R = -1. This result is achievable through the so-called Walker's method [35]. We also implemented a third different load ratio for R2 specimens to validate the results of the numerical simulations.

Furthermore, the fractography analysis is shown, with the goal of fully describing the behaviour of the material under fatigue loads.

4. Numerical Simulations

To generalise the experimental results, numerical analysis based on the finite element method (FEM) was carried out. The simulations were performed through the software Solidworks® (2024), and for the smooth specimen, a solid mesh of 86,315 quadratic tetrahedral elements (TET10) and 127,813 nodes was implemented, as shown in Figure 6a.

For the notched specimen, a solid mesh consisting of 163,583 quadratic tetrahedral elements (TET10) and 242,584 nodes was implemented, as shown in Figure 6b. Both final meshes resulted from an h-refinement process with a destination precision of 98%. This strategy implies progressively decreasing the characteristic size of the finite elements (denoted as h) in areas necessitating higher accuracy, typically guided by error estimators supplied by the solver. The target accuracy of 98% relates to the convergence criterion established in SolidWorks®, wherein the solver evaluates the outcomes of successive mesh refinements and assesses the percentage of convergence towards an asymptotic solution. A local mesh control was also applied around the hole, featuring an average element size of 0.1 mm, with an element size/diameter hole ratio equal to 1/20. This guaranteed that the stress gradients surrounding the geometric discontinuity were accurately captured with adequate resolution, enhancing the overall h-refinement strategy.

About the boundary conditions, to represent the actual behaviour of the specimen stressed on the experimental machine, Figure 6c shows where the fixed constraints (defined by green arrows) and the forces/displacements controlled (indicated by purple arrows) were applied. Due to this configuration, the mesh's refinement at the edge of the fixed constraint was justified; however, that area of the specimen was not the focus of this research study, as the gauge area was the one analysed.

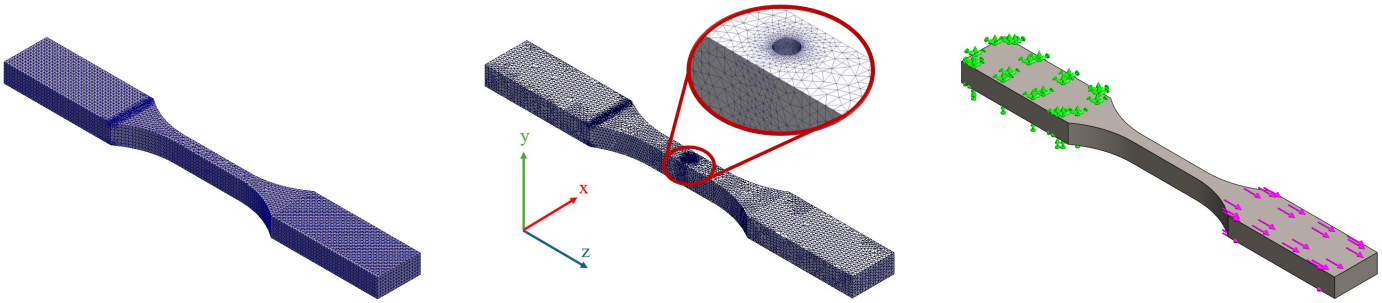

(**a**) (**b**) (**c**)

Figure 6. Meshes adopted. (**a**) Mesh of the smooth specimen. (**b**) Mesh of the notched specimen. (**c**) Image of the boundary conditions applied to the numerical simulations.

5. Results and Discussion

5.1. Results of Tensile Tests

Regarding the tensile tests, as previously explained, three specimens were tested. From the experimental results, the stress–strain curve of the material was derived and then implemented in the numerical simulations to analyse the notch behaviour.

5.1.1. Experimental Results of Tensile Tests

Table 5 enhances the data obtained from the tensile specimens and compares them with the supplier's data, while Figure 7 shows the tensile tests conducted. It is noticeable that the average of the values is higher than the declared values for every mechanical property analysed.

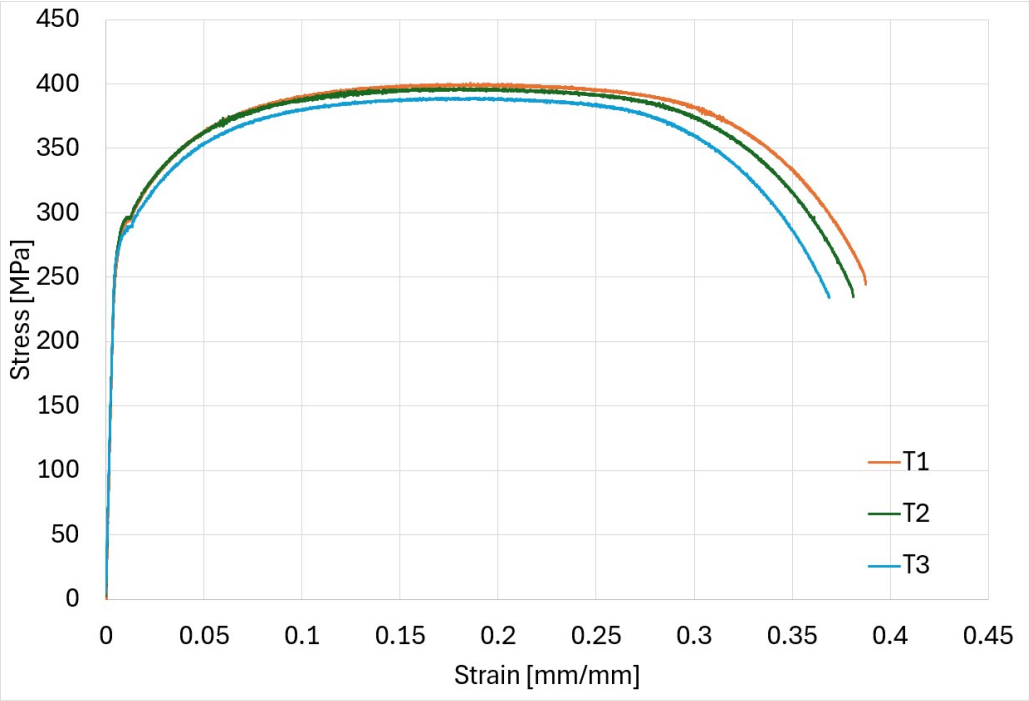

Figure 7. σ–ϵ charts of the tensile tests.

Table 5. Summary of the tensile tests results. The supplier values are in accordance with the UNI EN 10025-2 standard [36].

Specimen ID	E [MPa]	σ_y [MPa]	σ_r [MPa]
Supplier's values	207,000	278	391
T1	228,580	290.06	400.38
T2	212,578	294.28	396.71
T3	208,229	278.32	389.28
Mean	216,462	287.56	395.46
Std. Dev.	10,717	8.27	5.66

5.1.2. Numerical Results of Tensile Tests

For a better comprehension of the experimental tests, some numerical simulations were performed. One goal of this study was to extend the knowledge about the strength concentration factor; therefore, Figure 8 shows the numerical result for a linear static simulation of the notched specimen.

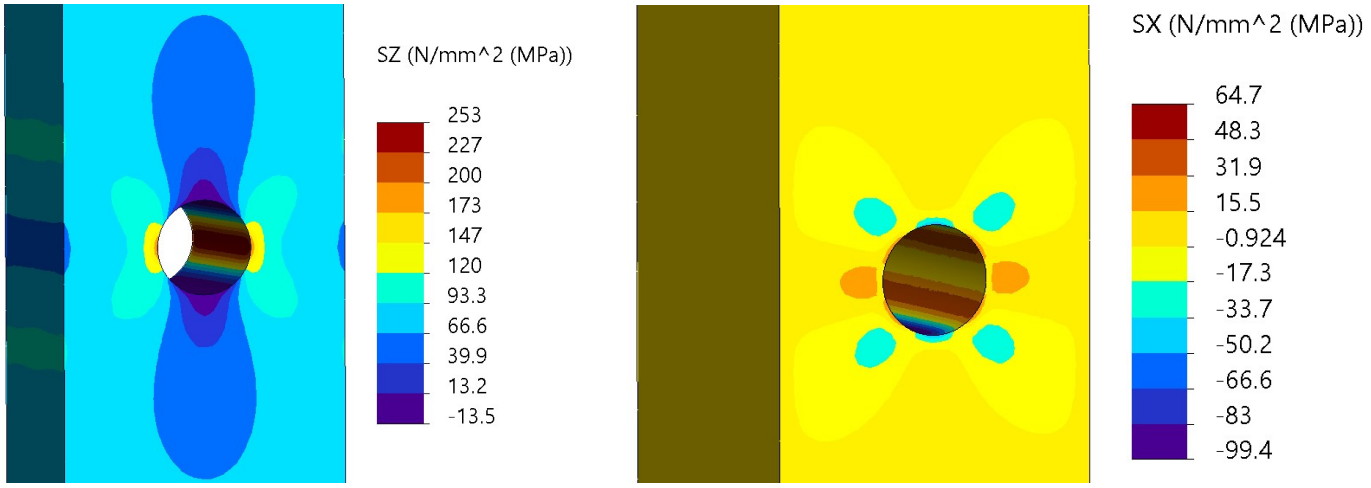

(**a**) (**b**)

Figure 8. FEM results in an elastic field for the notched specimen: the coordinate system is the same as in Figure 6b. (**a**) Stress results along the Z-axis. (**b**) Stress results along the X-axis. It is possible to notice that in the most stressed area around the hole, the stress along this axis is equal to zero, meaning that here there is a plane stress state, a condition confirmed in the literature [37].

The stress applied was through a tensional force equal to 3000 N in the elastic field of the material. On the smooth specimen, a stress value of 107 MPa was analytically evaluated (having a gauge area equal to 28 mm^2), while for the notched specimen, the value was 253 MPa, as it can be seen from the FEM results; the stress concentration factor K_t is defined in Equation (2) [38]:

$$K_t = \frac{\sigma_{max,n}}{\sigma_n} \tag{2}$$

where $\sigma_{max,n}$ is the value of the stress at the edge of the hole, and σ_n is the nominal stress calculated at a location without a hole. This value was equal to 2.36, which is in line with the value found in the literature [38,39] for the example of a finite-width plate with a circular hole.

5.2. Results of Fatigue Tests

5.2.1. Results for the Fatigue Behaviour of the Material

Regarding the fatigue tests, the first study concerned the behaviour of the material; Figure 9 hence displays HCF and staircase data along with the bilinear model that was inferred from it. The two thinner lines represent the *S*–*N* curves for 10% and 90% probabilities of failure with a confidence level of 95% [28].

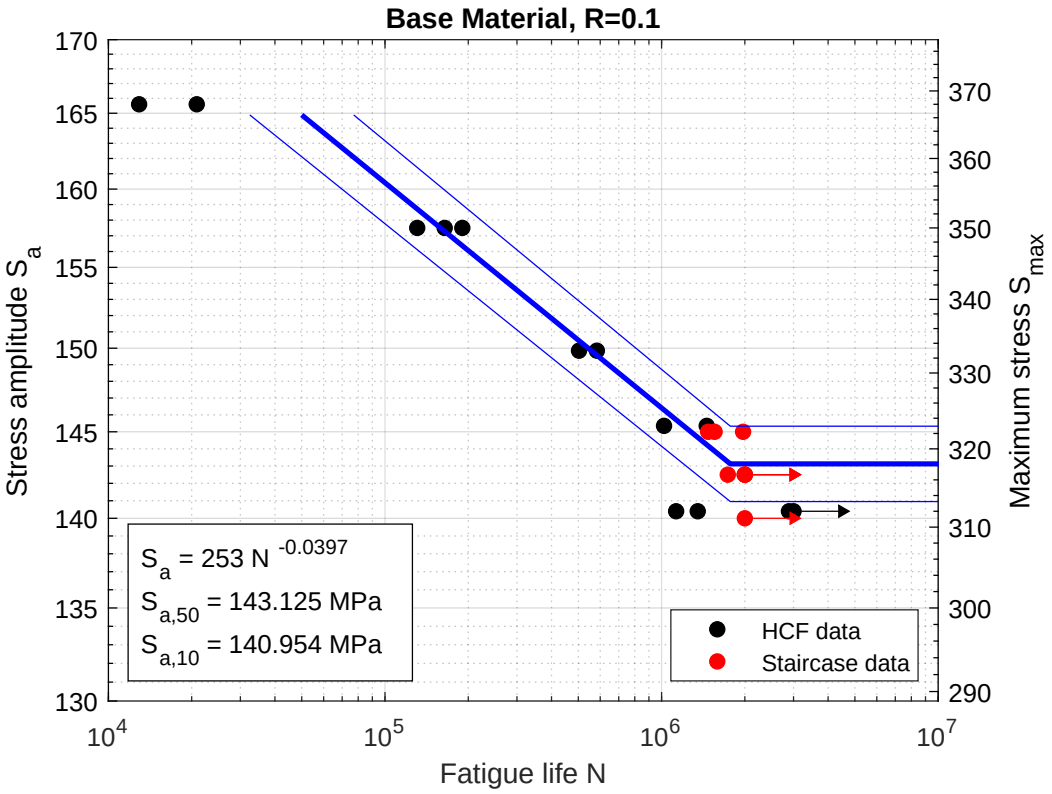

Figure 9. Full *S*–*N* curve of DD11 steel at a 0.1 stress ratio.The arrows show the runouts.

The stress–life curve inferred above was based on fatigue tests carried out at a stress ratio of 0.1, which means that every single test was characterised by a positive (hence, tensile) mean stress in addition to the pulsating component typical of fatigue. It is well known that a tensile mean stress has a detrimental effect on fatigue life, and a number of different methods exist to obtain the equivalent fully reversed fatigue strength when the stress ratio differs from -1 (i.e., the stress ratio of a traditional Wöhler curve).

In this work, as already mentioned in Section 3, the Walker method was adopted since it offers the advantage of a better fit of the data thanks to the experimental parameter γ, which can be interpreted as an indicator of the material's sensitivity to mean stresses in fatigue. The method is based on a bilinear regression of high-cycle fatigue data acquired at different stress ratios. Therefore, HCF tests at the stress ratios of 0.01 and 0.2 were carried out. As previously defined, the choice of these particular values was driven by the need to avoid compression and by a limitation on maximum stress to maintain the same failure mode and stay away from the LCF field, respectively.

A comprehensive stress–life plot of all the tests performed is available in Figure 10. It can be noted that the linear regression curves at 0.1 and 0.01 stress ratios feature similar slopes, which are quite different from the one at a ratio R = 0.2. This variation can be explained by the high maximum stresses and the main presence of the mean stress.

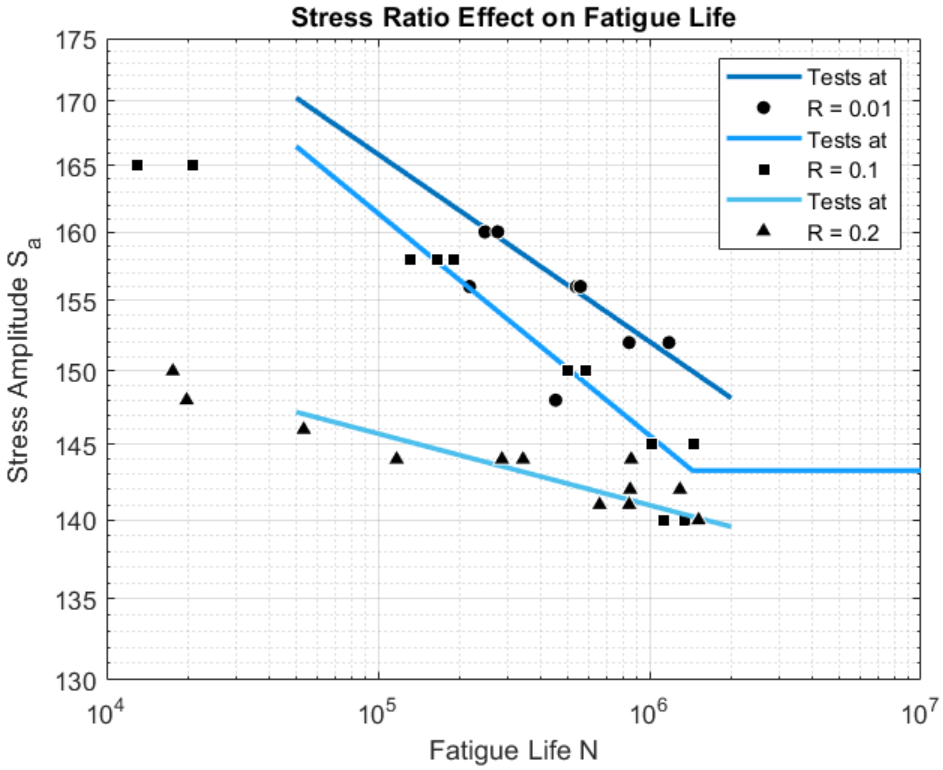

Figure 10. Comparison of experimental results and stress–life curves for different stress ratios. N.B.: staircase data and runouts in HCF tests are not displayed.

The next step was to apply the Walker equation: this equation correlates the equivalent fully reversed stress amplitude σ_{ar} with the actual parameters of a cycle. It can be expressed as Equation (3):

$$\sigma_{ar} = \sigma_{\max}^{1-\gamma}\,\sigma_a^{\gamma} = \sigma_a\left(\frac{2}{1-R}\right)^{1-\gamma} \tag{3}$$

and can be used to estimate the equivalent Wöhler curve based on fatigue tests carried out at load ratios other than -1. For fully reversed loading, the material is assumed to still follow the Basquin equation in HCF, as defined in Equation (4) [40]:

$$\sigma_{ar} = A_p\,N_f^{b} \tag{4}$$

Overall, the unknown parameters A, b and γ were found. The method involved a multiple linear regression, modelled as Equation (5):

$$y = m_1 x_1 + m_2 x_2 + d \quad where \quad y = \log N_f \tag{5}$$

Here, y is the dependent variable, while Equation (6) defines the independent variables:

$$x_1 = \log \sigma_{\max}\ ; \qquad x_2 = \log\left(\frac{1-R}{2}\right) \tag{6}$$

The fitting parameters are described in Equation (7). The regression was performed in Matlab®.

$$m_1 = \frac{1}{b} \qquad m_2 = \frac{\gamma}{b} \qquad d = -\frac{1}{b}\log A_p \tag{7}$$

Figure 11 displays the experimental points in the three-dimensional coordinate system (x_1, x_2, y) along with the planar surface that interpolates them. By rearranging the surface's parameters according to the above formulas, the values in Equation (8) were obtained:

$$\gamma = 0.5588\ ; \qquad \sigma_{ar} = 376\,N_f^{-0.0432} \tag{8}$$

Using Equation (8), it is possible to estimate the fatigue behaviour of the material with a stress ratio equal to -1 and thus the equivalent fully reversed fatigue limit, by evaluating that Basquin equation at the ultimate number of cycles of $2 \cdot 10^6$; the value is shown in Equation (9).

$$\sigma_{lim,R=-1} = 201\,\text{MPa} \tag{9}$$

To check these results, some numerical simulations were performed. Since the curve R = 0.2 was very different from the others, the fatigue analysis was based on using that stress ratio value. Figure 12 shows the fatigue behaviour for a finite life, with a linear regression defined by the Basquin equation and a confidence interval. It must be highlighted that this equation is valid only in HCF; for LCF values, the results can differ.

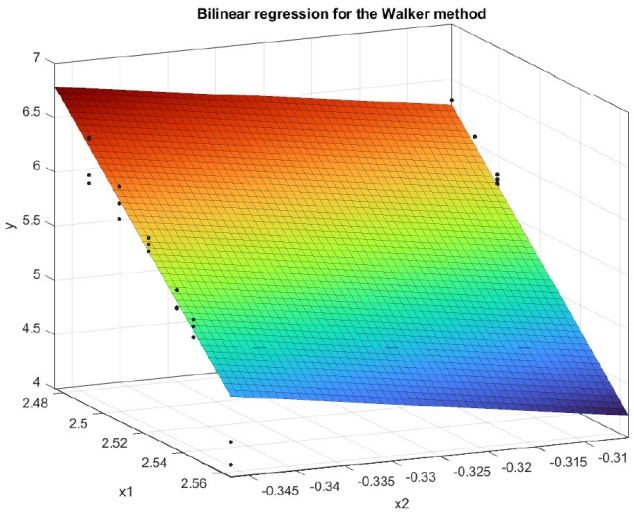

Figure 11. Graphical representation of the bilinear regression carried out for the Walker method. Here, the coefficient of determination is $R^2 = 0.9245$.

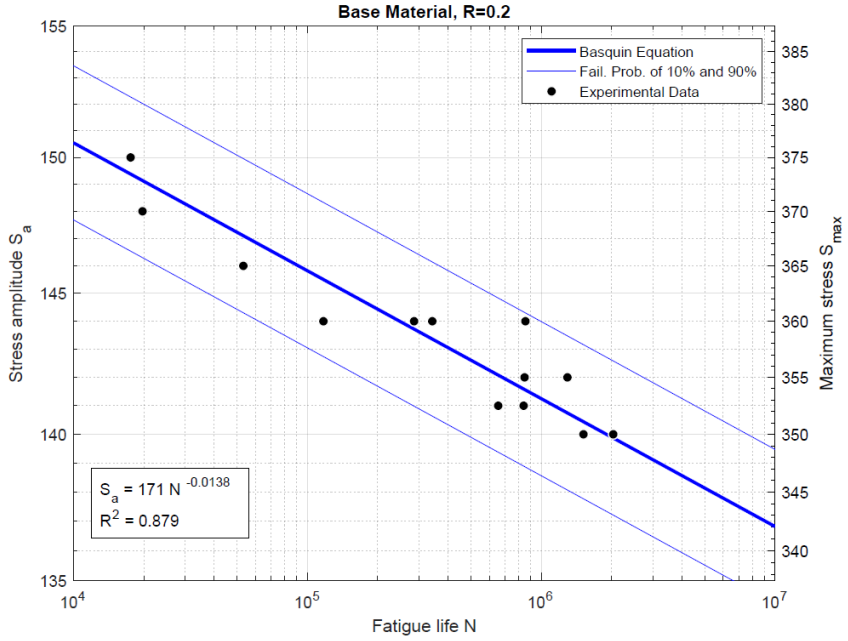

Figure 12. log–log stress–life plot of the HCF tests carried out at a 0.2 stress ratio.

A fatigue analysis was executed with $\sigma_a = 140$ MPa and another with $\sigma_a = 145$ MPa. The mean stress correction theory adopted in this research was Walker's method, as previously described. However, for the numerical simulations, the Wöhler curve was partially built

using the Basquin equation while remaining in the HCF area of the stress–life cycle plot, and the authors also tested whether other mean stress theories could be adopted.

Usually the literature indicates that experimental tests for ductile steel fall between Goodman's and Gerber's theory [41]. Here, the analysis showed that the Walker method was preferred for a number of cycles lower than 10^6 cycles, while the Goodman theory was a good choice for this material between 10^6 and $2 \cdot 10^6$ cycles (due to the experimental tests, the analysis stopped at that last value), indicating the minimum number of cycles required to reach failure inside the failure probability band of Figure 12. Specifically, in Figure 13, it is possible to see the results of this analysis, adopting the Goodman theory for the analysis performed at $\sigma_a = 140$ MPa and Walker's method for the analysis performed at $\sigma_a = 145$ MPa. In particular, it is possible to see the areas where the specimen reaches failure at the edge of the gauge length, as confirmed by the experimental results.

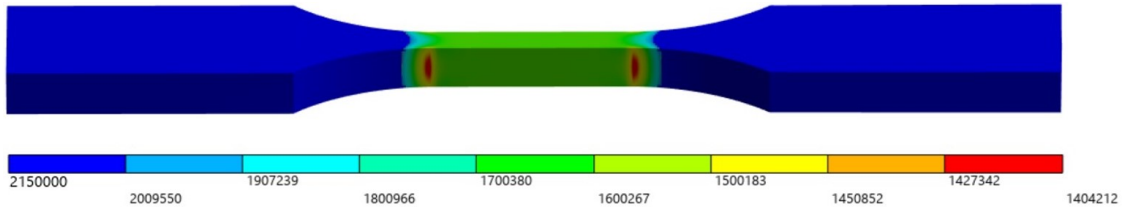

(**a**)

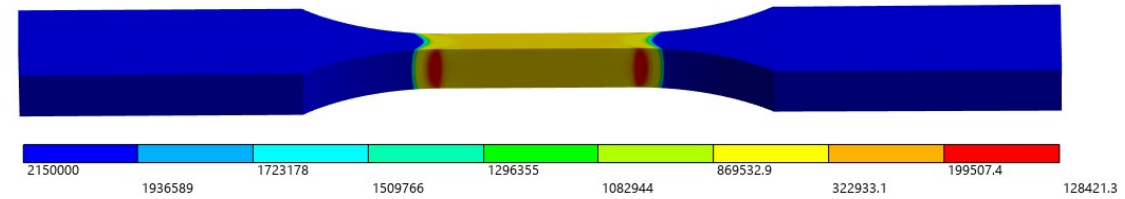

(**b**)

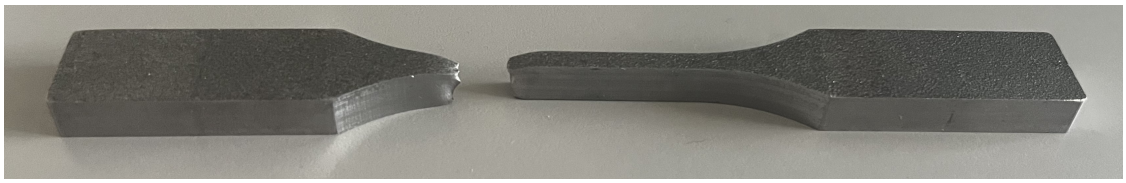

(**c**)

Figure 13. Fatigue analysis comparison. (**a**) FEM results in fatigue simulation: numerical results for the fatigue simulation with $R = 0.2$ and $\sigma_a = 140$ MPa. Here the number of cycles ranges from 2.15×10^6 to 1.4×10^6 cycles. (**b**) FEM results in fatigue simulation: numerical results for the fatigue simulation with $R = 0.2$ and $\sigma_a = 145$ MPa. Here the number of cycles ranges from 2.15×10^6 to 1.28×10^5 cycles. (**c**) Image of a specimen that reached failure; the failure area is in the same area found in the FEM results.

5.2.2. Results of Fatigue Limit for Pre-Stretched or Notched Specimens

Regarding the study of pre-strained specimens, a pre-strain level of tensile plastic deformation equal to 11% was applied to a group of smooth specimens so as to investigate the effect of pre-strain on the fatigue limit (as previously cited, a similar value of pre-strain was already investigated in the literature with a similar material [33]). In terms of stress, observing Figure 5b, it is possible to define a parameter χ in Equation (10):

$$\chi = \frac{\sigma_{ps,11\%}}{\sigma_y} = \frac{390 \text{ MPa}}{287 \text{ MPa}} = 1.36 \tag{10}$$

where $\sigma_{ps,11\%}$ is the stress to reach the level of plastic deformation equal to 11%, and σ_y is the yield stress of the material. The specimen identification for this group of specimens is referred to as PS. This level of pre-strain being located near the plateau of the σ–ε curve, the stretching process was conducted using displacement control.

For the notched tests, the fatigue limit was analysed.

Table 6 shows a comparison between all the fatigue limits analysed and the fatigue limit of the material. All the tests were conducted with a stress ratio of $R = 0.1$, but for the staircase method, different stress steps (ΔS) were adopted. The standards [28] highlight that if there is no information available about the standard deviation, a step of about 5% of the estimated mean fatigue strength may be used as the stress step. This means that the stress step for this material should be between 5 and 10 MPa. Experimentally, it was observed that having stress steps with these values was appropriate for the pre-stretched specimens with a high pre-deformation, but for the other tests, a value equal to 2.5 MPa could achieve a lower uncertainty of the results.

Table 6. Summary of the fatigue limits' results.

Specimen ID	$\sigma_{a,lim}$ [MPa]	Std. Dev. [MPa]	ΔS [MPa]
R1	143.25	0.77	2.5
PS	143.93	4.21	5
N	121.25	2.43	2.5

The values indicate that the pre-deformation of the specimen had an almost negligible effect on the fatigue limit, although there may be a slight increase in it. To strengthen this result, a non-linear numerical simulation for the pre-strain process was performed: Figure 14 shows the findings from the numerical simulation performed.

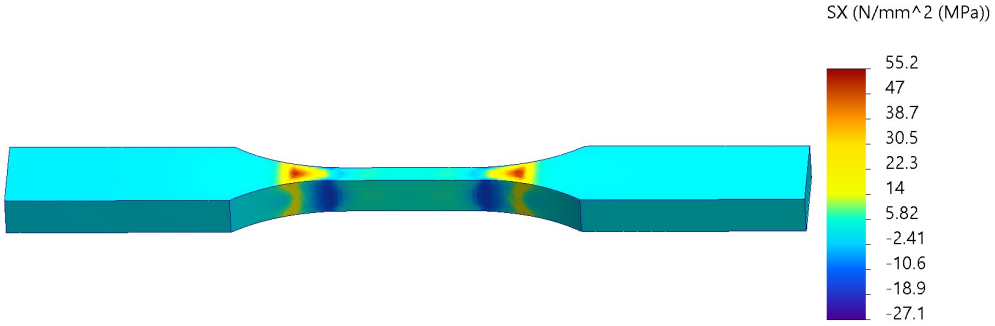

Figure 14. Numerical simulation results of the pre-strain phase.

The numerical results clearly show that the specimen presented some area on the gauge length with residual compression stress; this could explain the slight increment in the fatigue limit for the pre-strained specimens. Moreover, there was a residual tensile stress at the centre of the transition area, but due to the larger section, it did not affect the failure location of the specimen.

Comparing the fatigue limit of the material with the fatigue limit of the notched specimens, the fatigue strength concentration factor was analysed. Through Equation (11), it is possible to evaluate the fatigue notch factor K_f [42]:

$$K_f = \frac{\sigma_{a,lim,smooth}}{\sigma_{a,lim,notched}} \tag{11}$$

where $\sigma_{a,lim,smooth}$ is the unnotched fatigue limit of the material, and $\sigma_{a,lim,notched}$ is the fatigue limit of the notched material. We obtained K_f = 1.18.

To understand this result, the value of the fatigue notch sensitivity factor q should be evaluated through a material parameter defined as α in Equation (12):

$$\log \alpha = -1.079 \cdot 10^{-9}\sigma_r^3 + 2.740 \cdot 10^{-6}\sigma_r^2 - 3.740 \cdot 10^{-3}\sigma_r + 0.6404 \quad (12)$$

where R_m is the tensile strength of the material; this results in α equal to 0.339. With this value, it was then possible to evaluate the fatigue notch sensitivity factor q through Equation (13):

$$q = \frac{1}{1 + \sqrt{\frac{\alpha}{\rho}}} \quad (13)$$

where parameter α was computed previously, while ρ is the notch radius, that is, 1 mm in the geometry considered. This means a notch sensitivity factor q equal to 0.632. Considering the value of K_t, as described in Section 5.1, is equal to 2.36, an expected value of the elastic fatigue notch factor $K_{f,el}$ (the fatigue notch factor of the studied scenario if the stress cycle is under the yield strength of the material) can be obtained through Equation (14):

$$K_{f,el} = 1 + q \cdot (K_t - 1) = 1.85 \quad (14)$$

This result is much higher than the K_f value found experimentally. The reasons behind the decrease in the fatigue notch factor may be the stress conditions of the tests performed and the material used. As already seen in the literature [43–45], the decrease in K_f can be due to different factors:

- The stress ratio adopted ($R = 0.1$) and the loads applied bring the material in the elasto-plastic field;
- The material itself is very ductile, and combined with the geometry implemented, notch blunting phenomena can easily happen;
- Working in the high-cycle fatigue and very high cycle fatigue, repeated plastic strain accumulation can occur, avoiding the propagation of cracks.

In fact, considering that $\sigma_{a,lim}$ was evaluated to be 121.25 MPa for the notched specimen and the stress ratio R was equal to 0.1, through Equation (15), it was possible to evaluate the maximum stress during the fatigue limit cycle $\sigma_{max,lim}$:

$$\sigma_{max,lim} = \frac{2 \cdot \sigma_{a,lim}}{1 - R} = 269.44 \text{ MPa} \quad (15)$$

where R is the stress ratio. Thus, the maximum local stress could be evaluated through Equation (16) thanks to the stress concentration factor K_t:

$$\sigma_{max,loc} = K_t \cdot \sigma_{max,lim} = 633.19 \text{ MPa} > \sigma_y = 287.56 \text{ MPa} \quad (16)$$

This means a yielding around the notch area, the value of maximum local stress $\sigma_{max,loc}$ being greater than the yielding strength of the material σ_y. To be specific, since the so-called condition of reversed yielding is not satisfied, the actual condition is called initial yielding [46]. In this condition, the fatigue notch factor for mean stress k_{fm} can be defined by Equation (17):

$$k_{fm} = \frac{\sigma_y - K_t \cdot \sigma_{a,lim}}{|\sigma_{m,lim}|} = 0.018 \quad (17)$$

where $\sigma_{a,lim}$ and $\sigma_{m,lim}$ are the alternate and the mean stress of the notch fatigue limit cycle, respectively. This result describes an almost reversed yielding condition (where the fatigue notch factor for mean stress k_{fm} is equal to zero), yielding the following stresses on the notch area:

$$\sigma_{a,loc} = K_t \cdot \sigma_{a,lim} = 284.94 \text{ MPa}\,; \quad \sigma_{m,loc} = k_{fm} \cdot \sigma_{m,lim} = 2.66 \text{ MPa} \quad (18)$$

where the $\sigma_{a,loc}$ and $\sigma_{m,loc}$ are the alternate and the mean stress of the notch fatigue limit cycle localised in the plasticised area, respectively.

5.2.3. Fractography of Fatigue Tests

Figure 15 shows the fracture's surface of the specimens observed under each testing condition. In general, excluding the notched condition, two characteristic regions can be identified: the crack initiation and propagation area, which appears as a quarter-circle and lies on a single plane, and the final fracture region, inclined at approximately 45°, as typically observed in ductile materials. A schematic representation of the fracture surface highlighting these two regions is provided. The relative extension of these regions depends on the testing conditions. In particular, with an increasing stress ratio R, the extension of the propagation region decreases. This difference becomes significant starting from $R = 0.1$. The case of $R = 0.01$ shows only a slightly larger propagation zone compared to $R = 0.1$, while the difference between $R = 0.1$ and $R = 0.2$ is much more pronounced. The pre-strain condition shows only a slightly larger propagation region, which does not define a significant change in the material behaviour, as confirmed by the experimental results. Finally, in the notched condition, the presence of the hole masks any visible propagation effect on the fracture surface. The crack initiates directly from the hole surface, and the final fracture region resembles that of the unnotched specimens.

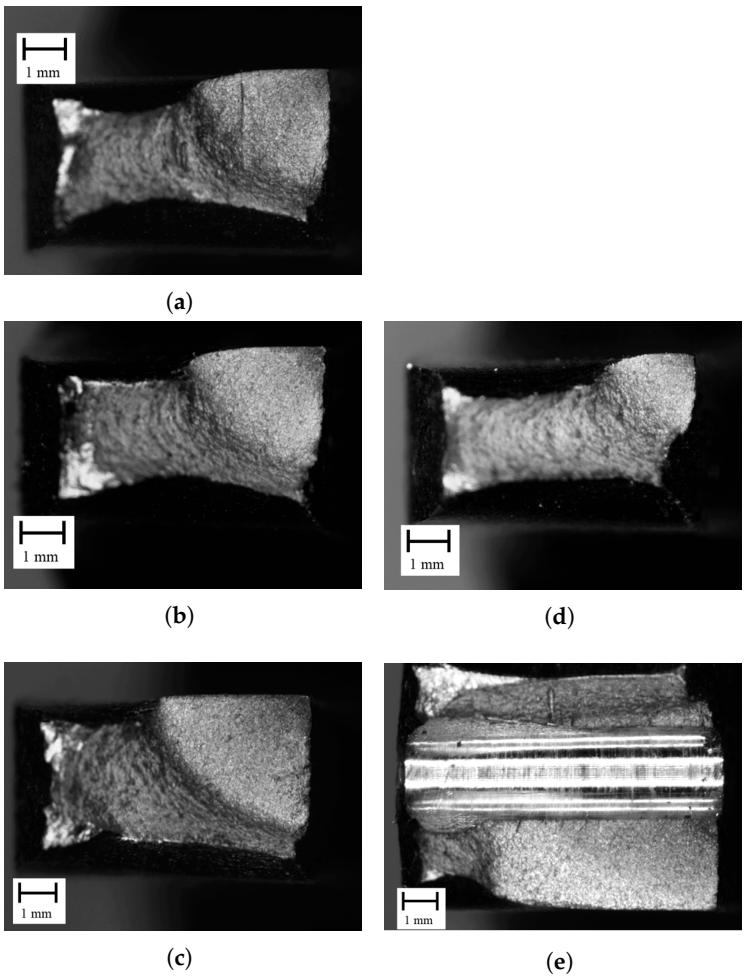

Figure 15. Images of the fracture surface of the specimens tested. (**a**) Fatigue specimen with $R = 0.01$. (**b**) Fatigue specimen with $R = 0.1$. (**c**) Fatigue specimen with a pre-strain value of $\epsilon_{res} = 11\%$ and $R = 0.1$. (**d**) Fatigue specimen with $R = 0.2$. (**e**) Fatigue specimen with a notch and $R = 0.1$.

6. Conclusions

This research study analysed the effect of pre-strain and notching on a flat steel bar made of DD11 low-carbon steel. After characterising the mechanical properties of the

material along the transversal direction (with respect to the rolling direction) and defining the fatigue behaviour of this material, two different conditions were analysed. The first one was the fatigue limit of the material with pre-strained specimens, where the residual level of pre-strain was equal to 11%, while the second condition was the fatigue limit of the material with notched specimens, with the aim of analysing the notch fatigue factor of the material with a stress ratio where the loads were greater than the yield strength. To understand the results obtained, numerical simulations were carried out, and documented photographs of the fracture area were taken. The following results were obtained:

- The concentration factor obtained from the numerical results was in line with the values defined in the scientific literature.
- A high pre-strain level had a negligible influence on the material's fatigue limit, indicating that even significant deformations (up to 11%) did not impact the material's fatigue performance.
- The notch factor found from the tests on notched samples indicated that the material was not very sensitive to fatigue, which is understandable because the material is very flexible and the stress ratio used in these tests increased the average stress. These testing conditions caused the material to behave like it was in an almost reversed yielding condition.

As future developments, fatigue limits with other levels of pre-strain can be studied to understand the fatigue behaviour of the material in different pre-strain conditions. The idea would be to analyse higher levels of pre-strain, even higher than the ultimate tensile strength point. Furthermore, the combination of pre-strain and notching can be analysed, with the aim of a better comprehension of the notching effect for this material. Other aspects that the authors would like to observe are methods for reducing the notching effect on the fatigue behaviour of the material.

Author Contributions: Conceptualization, G.D. and L.S.; methodology, L.S. and I.T.; software, L.S. and I.T.; validation, L.S. and I.T.; formal analysis, I.T. and C.P.; investigation, L.S.; resources, L.S. and A.M.; data curation, L.S., C.P. and A.M.; writing—original draft preparation, L.S. and I.T.; writing—review and editing, G.D. and L.S.; visualization, I.T. and C.P.; supervision, L.S.; project administration, G.D. and L.S.; funding acquisition, A.M. and L.S. All authors have read and agreed to the published version of the manuscript.

Funding: This research received no external funding.

Informed Consent Statement: Informed consent was obtained from all subjects involved in the study.

Acknowledgments: The authors would like to thank Silvio Bonometti for his valuable technical support. We also extend our gratitude to Moovero Company for providing the materials necessary for the experimental tests.

Conflicts of Interest: The authors declare no conflicts of interest.

Abbreviations

Symbol	Meaning	Symbol	Meaning
r	Radius [mm]	R	Stress ratio
σ_n	Stress amplitude [MPa]	σ_{max}	Maximum stress value of the stress oscillation
σ_{a50}	Lowest level of stress amplitude [MPa]	ΔS	Step level of the stress amplitude [MPa]
A	1st parameter of the staircase method	C	2nd parameter of the staircase method
B	3rd parameter of the staircase method	$Std.Dev.$	Standard deviation [MPa]
K_t	Stress concentration factor	$\sigma_{max,n}$	Stress at the edge of the hole [MPa]
σ_n	Nominal stress calculated at a location without a hole [MPa]	σ_{ar}	Fully reversed stress amplitude at N_f cycles [MPa]

Symbol	Meaning	Symbol	Meaning
γ	Walker's parameter	N_f	Fatigue life of the specimen [cycles]
A_p, b	Parameters for the Walker method	$\sigma_{lim,R=-1}$	Fully reversed fatigue limit [MPa]
χ	Loading pre-stress ratio	$\sigma_{ps,11\%}$	Stress ratio
E	Young's modulus [MPa]	σ_y	Yield strength [MPa]
σ_r	Tensile strength [MPa]	σ_y	Yield Strength [MPa]
$\sigma_{a,lim}$	Stress amplitude fatigue limit [MPa]	K_f	Fatigue notch factor
$\sigma_{a,lim,smooth}$	Unnotched fatigue limit [MPa]	$\sigma_{a,lim,smooth}$	Notched fatigue limit [MPa]
q	Notch sensitivity factor	α	Parameter for evaluation of q
ρ	Notch radius	$K_{f,el}$	Fatigue notch factor in elastic field
$\sigma_{max,lim}$	Maximum stress during fatigue limit cycle [MPa]	$\sigma_{max,loc}$	Maximum local stress during notch fatigue limit cycle [MPa]
K_{fm}	Fatigue notch factor for mean stress	$\sigma_{m,lim}$	Mean stress during notch fatigue limit cycle [MPa]

References

1. Matteis, P.; Scavino, G.; D'Aiuto, F.; Firrao, D. Fatigue Behavior of Dual-Phase and TWIP Steels for Lightweight Automotive Structures. *Steel Res. Int.* **2012**, *83*, 950–956. [CrossRef]
2. Kong, Y.S.; Abdullah, S.; Schramm, D.; Omar, M.Z.; Haris, S.M. Development of multiple linear regression-based models for fatigue life evaluation of automotive coil springs. *Mech. Syst. Signal Process.* **2019**, *118*, 675–695. [CrossRef]
3. Li, C.; Feng, Y.; Ding, K. Comparative research of lifting equipment fatigue life prediction based on different cumulative damage models. In Proceedings of the 2023 4th International Conference on Machine Learning and Computer Application, Hangzhou, China, 27–29 October 2023.
4. Fratila, C.; Axinte, T.; Cojocaru, R.C.; Berescu, C.; Scurtu, I.C. The study of the lifting mechanism of the crane arm to a barge. *Technium* **2020**, *2*, 91–96. [CrossRef]
5. Dong, Q.; Yang, P.; Xu, G.; Deng, J. Mechanisms and modeling of low cycle fatigue crack propagation in a pressure vessel steel Q345. *Int. J. Fatigue* **2016**, *89*, 2–10. [CrossRef]
6. Hu, Y.; Qin, Q.; Wu, S.; Zhao, X.; Wang, W. Fatigue resistance and remaining life assessment of induction-hardened S38C steel railway axles. *Int. J. Fatigue* **2021**, *144*, 106068. [CrossRef]
7. Noh, K.; Shams, S.A.A.; Kim, W.; Kim, J.N.; Lee, C.S. Influence of microstructure on low-cycle and extremely-low-cycle fatigue resistance of low-carbon steels. *Met. Mater. Int.* **2021**, *27*, 3862–3874. [CrossRef]
8. Bach, J.; Göken, M.; Höppel, H.-W. Fatigue of low alloyed carbon steels in the HCF/VHCF-regimes. In *Fatigue of Materials at Very High Numbers of Loading Cycles: Experimental Techniques, Mechanisms, Modeling and Fatigue Life Assessment*; Springer: Berlin/Heidelberg, Germany, 2018; pp. 1–23.
9. Kim, Y.; Hwang, W. High-cycle, low-cycle, extremely low-cycle fatigue and monotonic fracture behaviors of low-carbon steel and its welded joint. *Materials* **2019**, *12*, 4111. [CrossRef]
10. Tsutsumi, N.; Murakami, Y.; Doquet, V. Effect of test frequency on fatigue strength of low carbon steel. *Fatigue Fract. Eng. Mater. Struct.* **2009**, *32*, 473–483. [CrossRef]
11. Mayer, H. Fatigue damage of low amplitude cycles in low carbon steel. *J. Mater. Sci.* **2009**, *44*, 4919–4929. [CrossRef]
12. Le, Q.; Kang, H.T.; Kridli, G.; Khosrovaneh, A.K.; Yan, B. Effect of prestrain paths on mechanical behavior of dual phase sheet steel. *Int. J. Fatigue* **2009**, *31*, 607–615. [CrossRef]
13. Sivaprasad, S.; Tarafder, S.; Ranganath, V.R.; Ray, K.K. Effect of prestrain on fracture toughness of HSLA steels. *Mater. Sci. Eng. A* **2000**, *284*, 195–201. [CrossRef]
14. Robertson, L.T.; Hilditch, T.B.; Hodgson, P.D. The effect of prestrain and bake hardening on the low-cycle fatigue properties of TRIP steel. *Int. J. Fatigue* **2008**, *30*, 587–594. [CrossRef]
15. Kang, M.; Aono, Y.; Noguchi, H. Effect of prestrain on and prediction of fatigue limit in carbon steel. *Int. J. Fatigue* **2007**, *29*, 1855–1862. [CrossRef]
16. ASM Handbook Committee. *Volume 19: Fatigue and Fracture*; ASM International: Geauga County, OH, USA, 1996.
17. Liao, D.; Zhu, S.P.; Correia, J.A.F.O.; De Jesus, J.M.P.; Berto, F. Recent advances on notch effects in metal fatigue: A review. *Fatigue Fract. Eng. Mater. Struct.* **2020**, *43*, 637–659. [CrossRef]
18. Zhang, H.; Deng, Y.; Cao, Y.; Chen, F.; Luo, Y.; Xiao, X. Field testing, analytical, and numerical assessments on the fatigue reliability on bridge suspender by considering the coupling effect of multiple pits. *Struct. Infrastruct. Eng.* **2025**, 1–16. [CrossRef]
19. Zhang, H.; Liu, H.; Deng, Y.; Cao, Y.; He, Y.; Liu, Y.; Deng, Y. Fatigue behavior of high-strength steel wires considering coupled effect of multiple corrosion-pitting. *Corros. Sci.* **2025**, *244*, 112633. [CrossRef]

20. Zhang, H.; Deng, Y.; Chen, F.; Luo, Y.; Xiao, X.; Lu, N.; Liu, Y.; Deng, Y. Fatigue Life Prediction for Orthotropic Steel Bridge Decks welds Using a Gaussian Variational Bayes Network and Small Sample Experimental Data. *Reliab. Eng. Syst. Saf.* **2025**, *264*, 111406. [CrossRef]
21. Mazzoni, A.; Solazzi, L. Experimental field test on a multipiece steel wheel and influence of the material properties on its fatigue life evaluation. *Eng. Fail. Anal.* **2022**, *135*, 106106. [CrossRef]
22. Solazzi, L.; Mazzoni, A. Experimental study of the fatigue life of off-highway steel wheels using the rim section test approach. *Appl. Sci.* **2023**, *13*, 9119. [CrossRef]
23. *UNI EN 10027-2:2015*; Designation Systems for Steels—Part 2: Numerical System. Ente Nazionale Italiano di Unificazione (UNI): Milan, Italy, 2015.
24. *UNI EN 10111:2008*; Continuously Hot Rolled Low Carbon Steel Sheet and Strip for Cold Forming. Ente Nazionale Italiano di Unificazione (UNI): Milan, Italy, 2008.
25. *ISO 377:2017*; Steel and Steel Products—Location and Preparation of Samples and Test Pieces for Mechanical Testing. International Organization for Standardization (ISO): Geneva, Switzerland, 2017.
26. *UNI EN 10051:2024*; Lamiere e Nastri Laminati a Caldo in Continuo, Non Rivestiti, di Acciai Non Legati e Legati—Tolleranze Dimensionali e di Forma. Ente Nazionale Italiano di Unificazione (UNI): Milan, Italy, 2024.
27. *ISO 6892-1:2019*; Metallic Materials—Tensile Testing. International Organization for Standardization: Geneva, Switzerland, 2019.
28. *ISO 12107:2017*; Metallic Materials—Fatigue Testing—Axial-Strain-Controlled Method. International Organization for Standardization: Geneva, Switzerland, 2017.
29. Pang, J.C.; Li, S.X.; Wang, Z.G.; Zhang, Z.F. General relation between tensile strength and fatigue strength of metallic materials. *Mater. Sci. Eng. A* **2013**, *564*, 331–341. [CrossRef]
30. Akay, S.K.; Yazıcı, M.; Bayram, A.; Avinc, A. Fatigue life behaviour of the dual-phase low carbon steel sheets. *J. Mater. Process. Technol.* **2009**, *209*, 3358–3365. [CrossRef]
31. Curà, F.; Curti, G.; Sesana, R. A new iteration method for the thermographic determination of fatigue limit in steels. *Int. J. Fatigue* **2005**, *27*, 453–459. [CrossRef]
32. Laamouri, A.; Sidhom, H.; Braham, C. Evaluation of residual stress relaxation and its effect on fatigue strength of AISI 316L stainless steel ground surfaces: Experimental and numerical approaches. *Int. J. Fatigue* **2013**, *48*, 109–121. [CrossRef]
33. Zhao, L.-H.; Cai, H.-C.; Weng, S.; Zheng, S.-L. Effect of pre-strain on the fatigue behavior of SAPH440 steel. *Mater. Express* **2019**, *9*, 1001–1008. [CrossRef]
34. *UNI ISO 3800*; Dispositivi Filettati—Resistenza Alla Fatica—Metodo di Prova. Ente Italiano di Normazione (UNI): Milan, Italy, 2014.
35. Dowling, N.E.; Calhoun, C.A.; Arcari, A. Mean stress effects in stress-life fatigue and the Walker equation. *Fatigue Fract. Eng. Mater. Struct.* **2009**, *32*, 163–179. [CrossRef]
36. *UNI EN 10025-2:2019*; Hot Rolled Products of Structural Steels—Part 2: Technical Delivery Conditions for Non-Alloy Structural Steels. Ente Nazionale Italiano di Unificazione (UNI): Milan, Italy, 2019.
37. Anderson, T.L.; Anderson, T.L. *Fracture Mechanics: Fundamentals and Applications*; CRC Press: Boca Raton, FL, USA, 2005.
38. Pilkey, W.D.; Pilkey, D.F.; Bi, Z. *Peterson's Stress Concentration Factors*; John Wiley & Sons: Hoboken, NJ, USA, 2020.
39. Gebrehiwot, S.Z.; Remes, H.; Karttunen, A. A Stress concentration factor for interacting surface notch and subsurface hole. *Raken. Mek.* **2018**, *51*, 20–37. [CrossRef]
40. Liu, Y.B.; Li, Y.D.; Li, S.X.; Yang, Z.G.; Chen, S.M.; Hui, W.J.; Weng, Y.Q. Prediction of the S-N curves of high-strength steels in the very high cycle fatigue regime. *Int. J. Fatigue* **2010**, *32*, 1351–1357. [CrossRef]
41. Bader, Q.; Kadum, E. Mean stress correction effects on the fatigue life behavior of steel alloys by using stress life approach theories. *Int. J. Eng. Technol.* **2014**, *14*, 50–58.
42. Lee, Y.-L.; Barkey, M.E.; Kang, H.T. Stress-based uniaxial fatigue analysis. In *Metal Fatigue Analysis Handbook: Practical Problem-Solving Techniques for Computer-Aided Engineering*; Butterworth-Heinemann: Oxford, UK, 2011.
43. Liu, M.; De Oliveira Miranda, A.C.O.; Antunes, M.A.; Meggiolaro, M.A.; Castro, J.T.P. Plastic stress concentration effects in fatigue strength. *Int. J. Fatigue* **2023**, *168*, 107394. [CrossRef]
44. Kim, J.-S.; Larrosa, N.O.; Horn, A.J.; Kim, Y.-J.; Ainsworth, R.A. Notch bluntness effects on fracture toughness of a modified S690 steel at 150 °C. *Eng. Fract. Mech.* **2018**, *188*, 250–267. [CrossRef]
45. Kolasangiani, K.; Farhangdoost, K.; Varvani-Farahani, A. Ratcheting progress at notch root of 1045 steel samples over asymmetric loading cycles: Experiments and analyses. *Fatigue Fract. Eng. Mater. Struct.* **2018**, *41*, 1870–1883. [CrossRef]
46. Dowling, N.E.; Kampe, S.L.; Kral, M.V. *Mechanical Behavior of Materials*, 5th ed.; Pearson: London, UK, 2018.